Surface plasmon-coupled emission on plasmonic Bragg gratings

Mana Toma,[1,3] Koji Toma,[1,3] Pavel Adam,[2] Jiří Homola,[2] Wolfgang Knoll,[1] and Jakub Dostálek[1,*]

[1] *AIT - Austrian Institute of Technology GmbH, Muthgasse 11, 1190 Vienna, Austria*
[2] *Institute of Photonics and Electronics, Academy of Sciences CR, Chaberská 57, 18251 Prague, Czech Republic*
[3] *These authors contributed equally to this work*
[*] *jakub.dostalek@ait.ac.at*

Abstract: Surface plasmon-coupled emission (SPCE) from emitters in a close proximity to a plasmonic Bragg grating is investigated. In this study, the directional fluorescence emission mediated by Bragg-scattered surface plasmons and surface plasmons diffraction cross-coupled through a thin metallic film is observed by using the reverse Kretschmann configuration. We show that controlling of dispersion relation of these surface plasmon modes by tuning the refractive index at upper and lower interfaces of a dense sub-wavelength metallic grating enables selective reducing or increasing the intensity of the light emitted to certain directions. These observations may provide important leads for design of advanced plasmonic structures in applications areas of plasmon-enhanced fluorescence spectroscopy and nanoscale optical sources.

OCIS codes: (240.6680) Surface plasmons; (300.2530) Fluorescence, laser-induced; (050.1950) Diffraction gratings; (050.6624) Subwavelength structures.

References and links

1. H. Aouani, O. Mahboub, N. Bonod, E. Devaux, E. Popov, H. Rigneault, T. W. Ebbesen, and J. Wenger, "Bright unidirectional fluorescence emission of molecules in a nanoaperture with plasmonic corrugations," Nano Lett. **11**(2), 637–644 (2011).
2. L. Novotny and N. van Hulst, "Antennas for light," Nat. Photonics **5**(2), 83–90 (2011).
3. P. A. Hobson, S. Wedge, J. A. E. Wasey, I. Sage, and W. L. Barnes, "Surface plasmon mediated emission from organic light-emitting diodes," Adv. Mater. (Deerfield Beach Fla.) **14**(19), 1393–1396 (2002).
4. S. Wedge, A. Giannattasio, and W. L. Barnes, "Surface plasmon-polariton mediated emission of light from top-emitting organic light-emitting diode type structures," Org. Electron. **8**(2-3), 136–147 (2007).
5. T. Okamoto, J. Simonen, and S. Kawata, "Plasmonic crystal for efficient energy transfer from fluorescent molecules to long-range surface plasmons," Opt. Express **17**(10), 8294–8301 (2009).
6. J. R. Lakowicz, K. Ray, M. Chowdhury, H. Szmacinski, Y. Fu, J. Zhang, and K. Nowaczyk, "Plasmon-controlled fluorescence: a new paradigm in fluorescence spectroscopy," Analyst (Lond.) **133**(10), 1308–1346 (2008).
7. J. Dostálek and W. Knoll, "Biosensors based on surface plasmon-enhanced fluorescence spectroscopy," Biointerphases **3**(3), FD12–FD22 (2008).
8. W. L. Barnes, "Fluorescence near interfaces: the role of photonic mode density," J. Mod. Opt. **45**(4), 661–699 (1998).
9. G. W. Ford and W. H. Weber, "Electromagnetic interactions of molecules with metal surfaces," Phys. Rep. **113**(4), 195–287 (1984).
10. P. Andrew and W. L. Barnes, "Molecular fluorescence above metallic gratings," Phys. Rev. B **64**(12), 125405 (2001).
11. J. R. Lakowicz, J. Malicka, I. Gryczynski, and Z. Gryczynski, "Directional surface plasmon-coupled emission: a new method for high sensitivity detection," Biochem. Biophys. Res. Commun. **307**(3), 435–439 (2003).
12. W. Knoll, M. R. Philpott, and J. D. Swalen, "Emission of Light from Ag Metal Gratings Coated with Dye Monolayer Assemblies," J. Chem. Phys. **75**(10), 4795–4799 (1981).
13. R. M. Amos and W. L. Barnes, "Modification of spontaneous emission lifetimes in the presence of corrugated metallic surfaces," Phys. Rev. B **59**(11), 7708–7714 (1999).
14. K. Tawa, H. Hori, K. Kintaka, K. Kiyosue, Y. Tatsu, and J. Nishii, "Optical microscopic observation of fluorescence enhanced by grating-coupled surface plasmon resonance," Opt. Express **16**(13), 9781–9790 (2008).

#164156 - $15.00 USD Received 6 Mar 2012; revised 6 Apr 2012; accepted 15 May 2012; published 11 Jun 2012

15. S. C. Kitson, W. L. Barnes, and J. R. Sambles, "Surface-Plasmon Energy Gaps and Photoluminescence," Phys. Rev. B Condens. Matter **52**(15), 11441–11445 (1995).
16. M. Kreiter, S. Mittler, W. Knoll, and J. R. Sambles, "Surface plasmon-related resonances on deep and asymmetric gold gratings," Phys. Rev. B **65**(12), 125415 (2002).
17. S. Wedge and W. L. Barnes, "Surface plasmon-polariton mediated light emission through thin metal films," Opt. Express **12**(16), 3673–3685 (2004).
18. W. H. Weber and C. F. Eagen, "Energy transfer from an excited dye molecule to the surface plasmons of an adjacent metal," Opt. Lett. **4**(8), 236–238 (1979).
19. E. Matveeva, J. Malicka, I. Gryczynski, Z. Gryczynski, and J. R. Lakowicz, "Multi-wavelength immunoassays using surface plasmon-coupled emission," Biochem. Biophys. Res. Commun. **313**(3), 721–726 (2004).
20. K. Toma, J. Dostalek, and W. Knoll, "Long range surface plasmon-coupled fluorescence emission for biosensor applications," Opt. Express **19**(12), 11090–11099 (2011).
21. Y. Wang, J. Dostalek, and W. Knoll, "Magnetic nanoparticle-enhanced biosensor based on grating-coupled surface plasmon resonance," Anal. Chem. **83**(16), 6202–6207 (2011).
22. E. Kretschmann, "Die Bestimmung optischer Konstanten von Metallen durch Anregung von Oberflächenplasmaschwingungen," Z. Phys. **241**(4), 313–324 (1971).
23. E. D. Palik, *Handbook of Optical Constants of Solids* (Elsevier, 1998).
24. W. L. Barnes, T. W. Preist, S. C. Kitson, and J. R. Sambles, "Physical origin of photonic energy gaps in the propagation of surface plasmons on gratings," Phys. Rev. B Condens. Matter **54**(9), 6227–6244 (1996).
25. F. Romanato, L. Hong, H. K. Kang, C. C. Wong, Y. Zong, and W. Knoll, "Azimuthal dispersion and energy mode condensation of grating-coupled surface plasmon polaritons," Phys. Rev. B **77**(24), 245435 (2008).

1. Introduction

Surface plasmon-coupled emission (SPCE) is of great interest in various areas including nanoscale optical antennas [1, 2], organic light-emitting diodes [3, 4], dye lasers [5] and fluorescence spectroscopy [6, 7]. Surface plasmons (SPs) are electromagnetic waves which originate from collective oscillations of charge density at metallic surfaces. SPs exhibit tightly confined field profile which is associated with greatly enhanced photonic mode density (PMD) and intensity of electromagnetic field at a metallic surface. Therefore, light radiated by emitters in the vicinity of a metal can be trapped by SPs and the coupling of absorption and emission dipoles of emitters with SPs dramatically alters their characteristics including the excitation rate, lifetime, and quantum yield [8, 9].

In order to convert energy emitted to SPs back to light waves propagating away from the metal, approaches utilizing diffraction gratings [10] and the reverse Kretschmann configuration of attenuated total reflection (ATR) method [11] were most commonly used. The employment of relief diffraction gratings for the extraction of fluorescence light from a metallic surface was firstly reported by Knoll et al. [12]. In this and later experiments, the corrugated metallic surfaces with the period comparable with the wavelength were typically used in studies including plasmon-mediated emission decay kinetics [13], angular distribution of emitted light [14], and emitted wavelength spectrum [15]. These investigations were carried out for gratings supporting regular SPs as well as coupled surface plasmon modes including Bragg-scattered surface plasmons [15, 16] and long range and short range surface plasmons on thin metallic films in refractive index symmetrical geometry [5, 17]. Relief gratings with non-sinusoidal profile allow additional control of the interaction strength between emitters and SPs through surface plasmon Bragg-scattering and associated bandgap occurring in their dispersion relation [5, 15]. The surface plasmon bandgap was shown to decrease the intensity of fluorescence light emitted via surface plasmons [15] which was, for instance, proposed for selective cancelling of spontaneous emission in plasmonic lasers [5]. In addition, Bragg-scattered surface plasmons were investigated for spatially controlled photobleaching of dyes [16]. In the other common optical platform of SPCE utilizing reverse Krestchmann configuration of ATR, a thin metal layer on a flat high refractive index substrate is used. The light emission occurs via surface plasmons that are leaky into the substrate forms a characteristic SPCE cone propagating away from the metal film [18, 19]. The polar angle of the cone is defined by the surface plasmon resonance (SPR) condition and it depends on the wavelength [19]. The width of the SPCE cone depends on the losses of surface plasmons and it can be strongly decreased by using long-range surface plasmons [20].

#164156 - $15.00 USD Received 6 Mar 2012; revised 6 Apr 2012; accepted 15 May 2012; published 11 Jun 2012

In this paper, we extend studies in surface plasmon-coupled emission on structures that combine the reverse Kretschmann configuration of ATR and dense sub-wavelength metallic gratings. These gratings carry a thin metallic film and are designed to alter dispersion relation of surface plasmon modes by Bragg-scattering on individual metal interfaces as well as by diffraction cross-coupling of SPs through the metal film. We show that these modes can be engineered to efficiently collect the fluorescence light from emitters on the top of the metal film and direct the emission to specific azimuth and polar directions into high refractive index substrate below the metallic film. The used dense sub-wavelength diffraction gratings do not couple the fluorescence light to the medium above the metal film.

2. Materials and methods

2.1 Materials

Photoresist Microposit S1818-G2 was purchased from Micro Resist Technology GmbH (Germany). Metal ion containing developer AZ 303 was obtained from MicroChemicals GmbH (Germany). Polydimethylsiloxane (PDMS) prepolymer and its curing agent were from Dow Corning (SYLGARD® 184). Amonil MMS10 was purchased from AMO GmbH (Germany). Poly(methyl methacrylate) (PMMA) was from Sigma-Aldrich Handels (Austria) and 1,1'-dioctadecyl-3,3,3′,3′-tetramethylindodicarbocyanine, 4 chlorobenzene-sulfonate salt (DiD) were from Invitrogen (LifeTech Austria). DiD dye exhibits the absorption and emission wavelengths of λ_{ab} = 644 nm and λ_{em} = 665 nm, respectively, and it was dispersed at the concentration of 700 nM in a toluene with dissolved PMMA (1.4 wt.%).

2.2 UV-NIL preparation of relief gratings

Holography was used for the preparation of master gratings. A polished Schott SF2 glass substrate with spin-coated photoresist layer was exposed to the interference field of two coherent collimated beams emitted from a HeCd laser at the wavelength λ = 325 nm (IK3031R-C, Kimmon Koha, Japan). Afterwards, the gratings were etched with a developer AZ-303 diluted with distilled water (volume ratio 1:9), rinsed with water and dried. Master gratings with sinusoidal relief modulation period Λ = 225-230 nm and depths of d = 10 and 30 nm were prepared and characterized by atomic force microscopy (data not shown). UV-nanoimprint lithography was used to replicate the master gratings as we described previously [21]. Briefly, a relief master grating was casted to a PDMS stamp which was cured overnight at 60 °C. Afterwards, the PDMS stamp was detached from the master and placed onto about 100 nm thick layer of UV-curable polymer Amonil that was spin-coated on a glass substrate. Amonil film in contact with the PDMS stamp was crosslinked by UV light dose of 36 J/cm^2 at a wavelength of λ = 365 nm (Bio-Link 365, Vilber Lourmat, Germany) followed by the release of the PDMS stamp from cured replica grating.

2.3 Layer structures supporting surface plasmons

LaSFN9 glass (refractive index of n_1 = 1.84 at λ_{em}) and BK7 glass (refractive index of n_1 = 1.51 at λ_{em}) substrates with Amonil grating (refractive index of n_2 = 1.51 at λ_{em}) were successively coated by layers supporting surface plasmons and containing DiD dye, see Fig. 1. Firstly, Ta_2O_5 (refractive index of n_3 = 1.79 at λ_{em}) and gold (refractive index n_4 = 0.167 + 3.91i at λ_{em}) films were deposited on the Amonil surface by using magnetron sputtering (UNIVEX 450C, Leybold Systems, Germany). The thickness of the gold film was set to 47 nm which is close to that providing the maximum strength of the coupling between surface plasmons and propagating waves in the glass substrate based on the Kretschmann configuration [22]. Afterwards, a 40 nm thick PMMA film (refractive index n_5 = 1.49 at λ_{em}) doped with DiD dyes was spin-coated on the gold surface and dried overnight at the room temperature. The PMMA surface was brought in contact with water (refractive index n_6 = 1.33 at λ_{em}) or air (refractive index n_6 = 1 at λ_{em}) in order to tune the propagation constant of

#164156 - $15.00 USD Received 6 Mar 2012; revised 6 Apr 2012; accepted 15 May 2012; published 11 Jun 2012

surface plasmons at the outer metal surface (SP_{outer}). The propagation constant of surface plasmons on the inner metallic surface (SP_{inner}) was varied by tuning the thickness of Ta_2O_5 layer t_3. Let us note that the Ta_2O_5 layer was deposited only on the LaSFN9 glass substrates with Amonil grating.

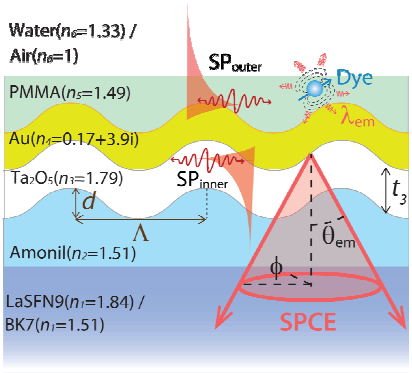

Fig. 1. Diffraction grating supporting surface plasmons that serve as emission channels for DiD dyes dispersed in a PMMA layer. Refractive indices of layers at the wavelength λ_{em} = 670 nm are shown for each layer.

3. Optical setup

Dispersion relation of surface plasmon modes on metallic grating surfaces was observed from angular reflectivity spectra R measured as a function of angle of incidence θ_I and wavelength λ. As seen in Fig. 2(a), a setup based on attenuated total reflection (ATR) method with Kretschmann configuration was used. A polychromatic beam from a halogen lamp (LSH102, LOT-Oriel, Germany) was coupled into an optical fiber (M25L02, Thorlabs, Germany), colimated with a lens (14 KLA 001, fl = 60 mm, CVI Melles Griot, Germany) and launched to a 90° glass prism that was made of identical glass as the grating sample substrate. At the prism base, the sample with a metallic grating was optically matched with a defined azimuth angle ϕ between the plane of incidence and grating vector **G**. The reflected light beam was coupled to an optical fiber and analyzed with a spectrometer (HR4000, Ocean Optics, USA). The prism and detectors were mounted on a two-circle rotation stage (Huber GmbH, Germany) in order to control the angle of incidence θ_I of the polychromatic beam in the prism. The data aquisition and control of the setup were supported by a home-built LabVIEW-based software. The reflectivity R was measured for transverse magnetic polarized incident beam (TM) and normalized with that measured for transverse electric polarization (TE).

#164156 - $15.00 USD Received 6 Mar 2012; revised 6 Apr 2012; accepted 15 May 2012; published 11 Jun 2012

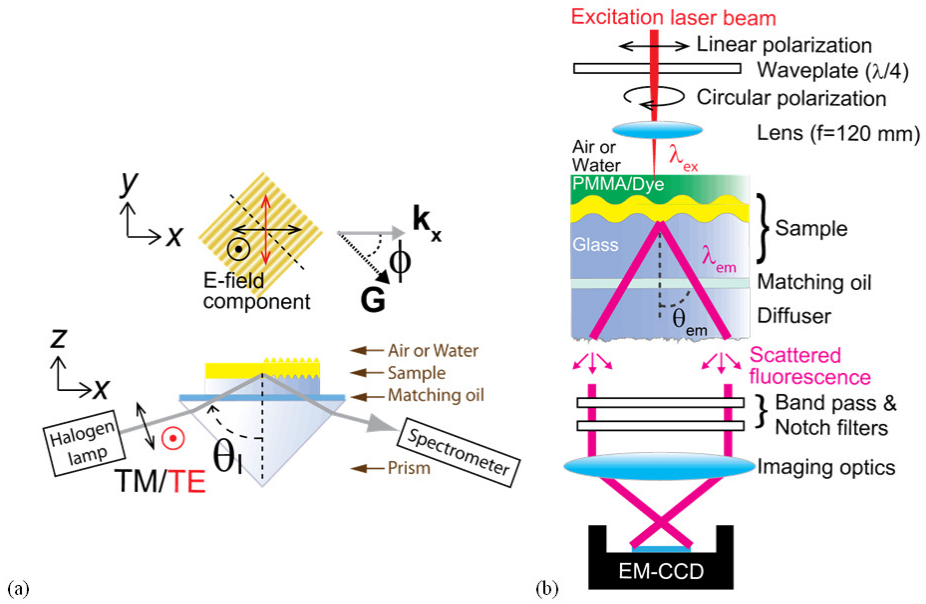

Fig. 2. Optical setup used for the measurement of (a) reflectivity spectra R as a function of angle of incidence θ_I, polar angle ϕ, and wavelength λ and (b) spatial distribution of surface plasmon-coupled emission in the glass substrate.

The measurement of spatial distribution of fluorescence intensity F emitted via surface plasmons into a glass substrate was carried out by using the setup depicted in Fig. 2(b). A sample with a metallic grating carrying a PMMA layer doped with a DiD dye was optically matched to a diffuser with rough bottom interface. Linearly polarized HeNe laser beam with the wavelength of λ = 632.8 nm that is close to the absorption wavelength of DiD dye λ_{ab} = 644 nm was circularly polarized by a quater waveplate (WPMQ05M-633, Thorlabs, Germany) and focused with a lens on the area of the surface of the structure with a diameter of about 100 μm. The fluorescence light coupled to surface plasmon modes at the emission wavelength λ_{em} of DiD dyes was re-radiated through the metal film based on the reverse Kretschamnn configuration, propagated through the substrate, and was scattered at the rough bottom surface of a diffuser made of LaSFN9 or BK7 glass. The spatial distribution of scattered fluorescence light was imaged onto an electron multiplying charge-coupled device (EM-CCD iXon + 885, Andor Technology, Ireland) by a camera lens (UNIFOC 58, Schneider Kreuznach, Germany). A set of filters including notch filter (XNF-632.8-25.0M, CVI Melles Griot, Germany) and band-pass filter (670FS10-25, LOT-Oriel, Germany) was used to reduce the background signal originating from the scattered and transmitted light at the excitation wavelength. The dependence of fluorescence signal on the polar angle θ_{em} in the glass substrate and azimuth angle ϕ was obtained from aquired fluorescence images. The central part of the image where the incident laser beam partially transmitted through the metal film was cut out by image processing as used filters did not suppress it totally.

4. Results and discussion

4.1 Surface plasmon-coupled emission on flat surface

The Bragg grating depicted in Fig. 1 supports surface plasmons at inner and outer interfaces of the metallic film. These modes act as pathways for fluorescence emission from dyes dispersed in the PMMA layer on the top of the gold film. Based on the Chance, Prock, and Silbey (CPS) model [9], we calculated the average energy dissipation density $dP/dk_{//}$ from an ensemble of dyes represented as randomly oriented dipoles. The energy dissipation density

#164156 - $15.00 USD Received 6 Mar 2012; revised 6 Apr 2012; accepted 15 May 2012; published 11 Jun 2012

for homogenously distributed dipoles in PMMA layer with the thickness of 40 nm was obtained by the averaging over distance from the metal surface between 0 and 40 nm as described in our previous work [20]. These simulations were carried out for flat layers (modulation depth d = 0 nm) shown in Fig. 1 with refractive indices taken from literature [23]. The results presented in Fig. 3 show $dP/dk_{//}$ as a function of in-plane component of the propagation constant $k_{//}$ of optical waves emitted from a dipole. $k_{//}$ is normalized by the propagation constant in vacuum k_0. They reveal that the coupling of fluorescence to surface plasmons at inner interface SP_{inner} (with the magnitude of propagation constant $k_{SPinner}$ = $|\mathbf{k}_{SPinner}|$) and outer interface SP_{outer} (with the magnitude of propagation constant $k_{SPouter}$ = $|\mathbf{k}_{SPouter}|$) is manifested as two distinct peaks. The probability of the emission via surface plasmons at inner and outer interfaces was calculated by integrating the energy dissipation density $dP/dk_{//}$ across respective peaks. For the layer architecture with 100 nm thick Ta_2O_5 on LaSFN9 glass and refractive index of the upper medium of n_6 = 1.33, 54 and 7% of emission events occurred via SP_{outer} and SP_{inner}, respectively. The fluorescence emission probability via SP_{outer} and SP_{inner} was redistributed to 40 and 14%, respectively, on the layer architecture consisting of BK7 glass without Ta_2O_5 layer. For both geometries, the peak energy dissipation density for the outer surface plasmon SP_{outer} is higher than that for the inner surface plasmon SP_{inner} due to the stronger overlap of SP_{outer} field with PMMA layer containing DiD dyes. The peak energy dissipation density for SP_{inner} is higher for the layer structure with BK7 substrate without Ta_2O_5 layer because its magnitude of propagation constant $k_{SPinner}$ is lower and thus larger portion of its field is carried in the PMMA layer. The fluorescence signal emitted via outer surface plasmon SP_{outer} can be recovered by the reverse Kretschmann configuration of ATR while that emitted via the inner surface plasmons SP_{inner} requires other means – e.g. diffraction grating. These simulations take into account fluorescence quenching due to the coupling to surface lossy waves with large propagation constant [9] ($k_{//}$ from 0 to 15k_0 was assumed in the model). This coupling is highly dependent on the distance from the metal surface. The majority of emission events is quenched below a characteristics length of about 15 nm which is smaller than the thickness of PMMA layer with dispersed DiD dyes.

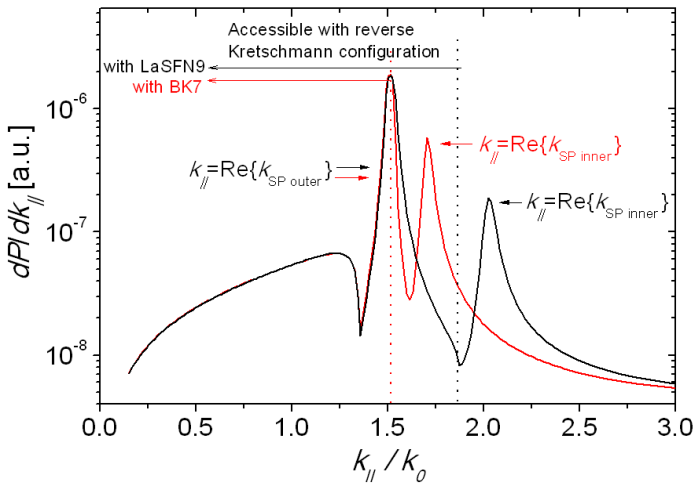

Fig. 3. Simulated average energy dissipation density $dP/dk_{//}$ of dyes dispersed in the 40 nm thick PMMA layer on the top of gold film with (t_3 = 100 nm, black line) or without (t_3 = 0 nm, red line) Ta_2O_5 layer. LaSFN9 (black line) and BK7 (red line) substrates were assumed. The PMMA layer is in contact with water (n_6 = 1.33).

4.2 Surface plasmon modes on corrugated metallic surfaces

On a corrugated layer structure, the characteristics of inner surface plasmons SP_{inner} and outer surface plasmons SP_{outer} are altered due to the interaction with the grating momentum $|\mathbf{G}|$ =

#164156 - $15.00 USD Received 6 Mar 2012; revised 6 Apr 2012; accepted 15 May 2012; published 11 Jun 2012

$2\pi/\Lambda$. In order to investigate changes in SP_{inner} and SP_{outer} modes, numerical simulations were carried out by using finite element method (FEM) implemented in a diffraction grating solver DiPoG (Weierstrass Institute, Germany). Figure 4(a) shows an example of the simulated dispersion relation of surface plasmon in the dependence of the reflectivity R on the angle of incidence θ_I and wavelength λ. For the grating structure with the modulation depth of d = 30 nm, Ta_2O_5 layer thickness of t_3 = 100 nm, and the refractive index of the upper medium n_6 = 1.33, the dispersion relation of SP_{outer} (at angles θ_I > 47 deg) is split in the vicinity to the wavelength of λ = 670 nm at which the grating momentum **G** matches the $2\mathbf{k}_{\mathbf{SPouter}}$. In this region, the counter-propagating SP_{outer} are Bragg scattered [24], which gives rise to a bandgap in their dispersion relation. At edges of the bandgap, Bragg-scattered surface plasmon modes (BSSPs) can be excited at wavelengths of λ = 630 nm and 730 nm. These SP_{outer} modes are referred as to ω^+ mode (λ = 630 nm) and ω^- mode (λ = 730 nm) and they exhibit electric field intensity localized at grating peaks (ω^-) and valleys (ω^+) as seen in Fig. 5(a) and 5(b), respectively. Let us note that the electric field intensity profiles are normalized with the maximum intensity $|\mathbf{E}_{\mathbf{max}}|^2$ to clarify the field distribution of considered plasmon modes. The increased PMD on the grating surface occurs at wavelengths where BSSPs can be excited as these modes are less dependent on the angle of incidence θ_I than regular surface plasmons, see Fig. 4. An additional resonance due to the −1st order diffraction grating coupling to surface plasmons at the inner surface of the gold film ($G\text{-}SP_{inner}$) is observed in Fig. 4(a). This resonance is associated with the field enhancement at the inner interface of the gold film as confirmed by the electric field intensity distribution presented in Fig. 5(c). $G\text{-}SP_{inner}$ resonance crosses over the SP_{outer} dispersion relation at wavelengths λ around 800 nm. When decreasing the thickness of Ta_2O_5 layer t_3, the momentum of SP_{inner} decreases and the resonance wavelength for the excitation of $G\text{-}SP_{inner}$ is blue-shifted. For the layer structure with Ta_2O_5 layer thickness of t_3 = 0 nm, $G\text{-}SP_{inner}$ resonance overlaps with the bandgap in SP_{outer} dispersion relation, see Fig. 4(b). The electric field intensity profile for $G\text{-}SP_{inner}$ inside the bandgap is presented in Fig. 5(d) and it shows this mode is partially coupled to SP_{outer} and exhibits a BSSP ω^+ nature at both inner and outer metallic interfaces. We assume that it originates from diffraction coupled counter-propagating SP_{outer} and SP_{inner} when $\mathbf{k}_{\mathbf{SPouter}} = \mathbf{G}\text{-}\mathbf{k}_{\mathbf{SPinner}}$ holds.

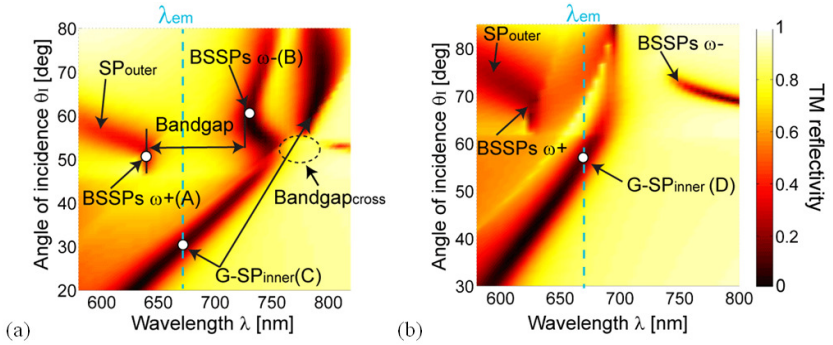

Fig. 4. Simulated reflectivity for grating modulation depth d = 30 nm and Ta_2O_5 layer with the thickness of (a) t_3 = 100 nm and (b) t_3 = 0 nm. The reflectivity (a) was calculated for LASFN9 substrate and (b) for BK7 substrate. Water on the top of PMMA layer and the azimuth angle ϕ = 0 deg are assumed.

#164156 - $15.00 USD Received 6 Mar 2012; revised 6 Apr 2012; accepted 15 May 2012; published 11 Jun 2012

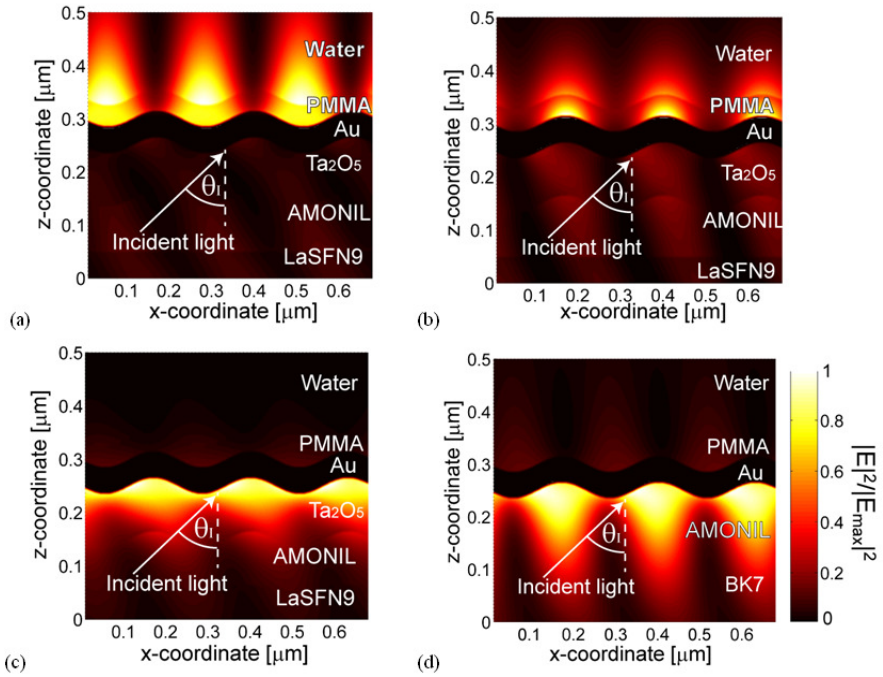

Fig. 5. Electric field intensity across the Bragg grating $|E|^2$ normalized with the maximum intensity $|(\mathbf{E})_{max}|^2$ calculated for (a) ATR–coupled BSSP mode ω^+ and (b) ATR–coupled BSSP mode ω^- at the outer gold interface, (c) grating-coupled propagating SP at the inner gold interface, and (d) coupled surface plasmon at the inner and outer interfaces. The respective angles and wavelengths are noted as circles in Fig. 4.

4.3 SPCE mediated by regular surface plasmons

SPCE on a flat layer structure without the corrugation (d = 0 nm) and air on the top (n_6 = 1) was firstly examined. The measured dispersion relation of surface plasmons for this geometry is shown in Fig. 6(a). It reveals that SPR occurs at the angle θ_l~39 deg in the LaFN9 glass substrate for the emission wavelength λ_{em} = 670 nm. The fluorescence image presented in Fig. 6(b) exhibits the characteristic SPCE cone with the polar angle θ_{em}~38 deg which is in agreement with the SPR condition at the emission wavelength λ_{em} in Fig. 6(a).

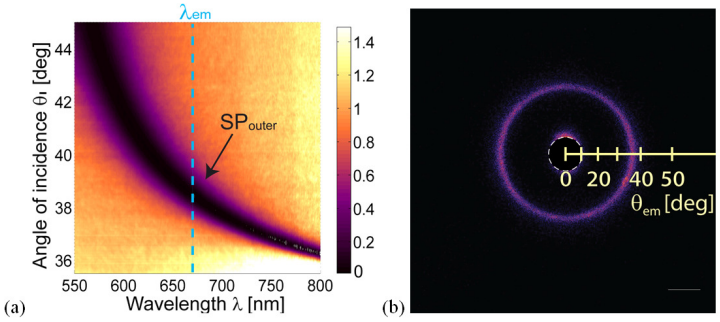

Fig. 6. (a) Dispersion relation of surface plasmons and (b) corresponding fluorescence emission image for flat layer structure on LaSFN9 substrate without Ta_2O_5 layer (t_3 = 0 nm) and air on the top n_6 = 1.

#164156 - $15.00 USD Received 6 Mar 2012; revised 6 Apr 2012; accepted 15 May 2012; published 11 Jun 2012

4.4 SPCE mediated by Bragg-scattered surface plasmons

Further, we investigated the effect of a Bragg grating to fluorescence emission on the samples supporting BSSPs modes close to the emission wavelength λ_{em}. When the refractive index of the upper medium is increased to n_6 = 1.33 and the layer structure is corrugated with the modulation depth of d = 10 nm, the resonant coupling to SP_{outer} shifts to higher angles and a gap appears in their dispersion relation. As seen in Fig. 7(a), BSSP modes located at edges of the bandgap occur at wavelengths of λ = 670 nm (ω^+) and 700 nm (ω^-). The BSSP ω^+ wavelength matches the fluorescence emission wavelength λ_{em} which leads to additional confinement of fluorescence signal on the SPCE cone at azimuth angles close to ϕ = 0 and 180 deg, see Fig. 7(b). The peak intensity at these angles where emission via BSSP ω^+ occurs was increased by a factor of ~3 compared to that for regular SPCE cone. This effect is due to the enhanced PMD associated with the presence of BSSP at the emission wavelength λ_{em} [24]. The emission via BSSPs occurs only at narrow range of azimuth angles as the bandgap is blue-shifted away from the emission wavelength λ_{em} by increasing ϕ. When increasing the modulation depth to d = 30 nm, the bandgap becomes wider and BSSP ω^+ and ω^- modes shifts to the wavelengths of 625 nm and 730 nm, respectively [see Fig. 7(c)] which agrees well with simulations presented in Fig. 4(a). Small differences between measured and simulated dispersion relation can be attributed to the discrepancy in refractive indices of materials and possible changes in modulation depth of the replicated grating. For this sample, the emission wavelength λ_{em} lies inside the bandgap and thus SPCE signal is canceled in the direction ϕ = 0 and 180 deg as shown in Fig. 7(d). Interestingly, the intensity of whole SPCE cone associated with emission via SP_{outer} modes is strongly decreased and the intensity of fluorescence signal at smaller polar angles θ_{em} is dramatically enhanced. This emission pattern is not symmetrical and the maximum intensity is observed at azimuth angles ϕ~ ± 50 and ± 130 deg.

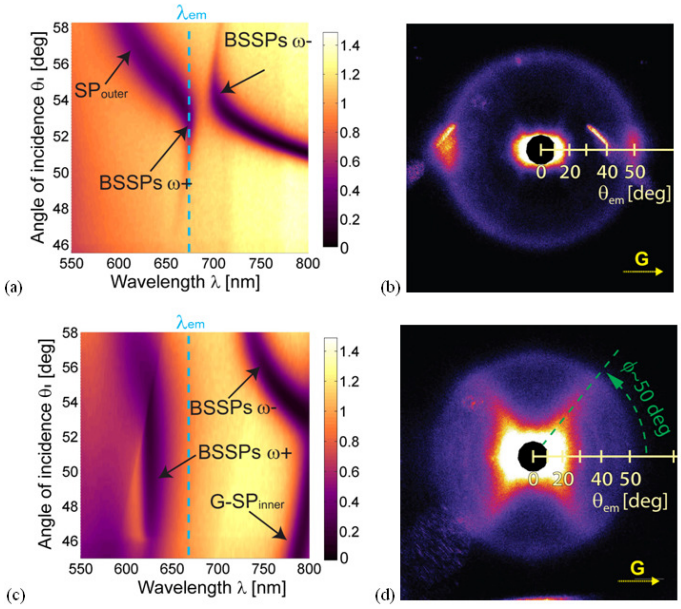

Fig. 7. Dispersion relations of surface plasmon modes on a gold grating surface with the Ta_2O_5 layer (t_3 = 100 nm) and water on the top (n_6 = 1.33) for the modulation depth of (a) d = 10 nm and (c) d = 30 nm. Corresponding spatial distribution of fluorescence light emitted into a LaSFN9 glass substrate for grating with the modulation depth of (b) d = 10 nm and (d) d = 30 nm.

In order to elucidate the origin of this feature, dispersion relation of surface plasmon modes supported by the grating was measured for azimuth angles varied from ϕ = 0 to 90 deg.

#164156 - $15.00 USD Received 6 Mar 2012; revised 6 Apr 2012; accepted 15 May 2012; published 11 Jun 2012

As shown in Fig. 8(a)-8(d), the wavelength at which G-SP_{inner} occurs is gradually blue-shifted and become less dependent on the angle of incidence θ_1 when increasing the azimuth angle ϕ. This observation agrees with previously reported works [25]. The measured azimuthal dispersion indicates that the the resonant coupling to G-SP_{inner} occurs at the emission wavelength of DiD dye λ_{em} = 670 nm for the azimuth angle ϕ = 50 deg. This angle matches the one at which the enhanced fluorescence emission was observed in Fig. 7(d). The weak dependence of the resonant wavelength on the angle of incidence θ_1 explains the broad polar angular range at which the fluorescence light is emitted via G-SP_{inner}. These data reveal that SP_{inner} can efficiently collect fluorescence light from fluorophores placed at the outer metallic surface. This feature is interesting as the simulated probability of the fluorescence emission for SP_{inner} on a flat structure is 6 times smaller than that for SP_{outer} (see Fig. 3) due to the relatively small overlap of SP_{inner} field with the top PMMA layer containing dyes [see Fig. 5(c)]. The enhanced emission rate via SP_{inner} can be ascribed to the redistribution of fluorescence emission pathways associated with the cancelling SP_{outer} on the corrugated grating layer architecture.

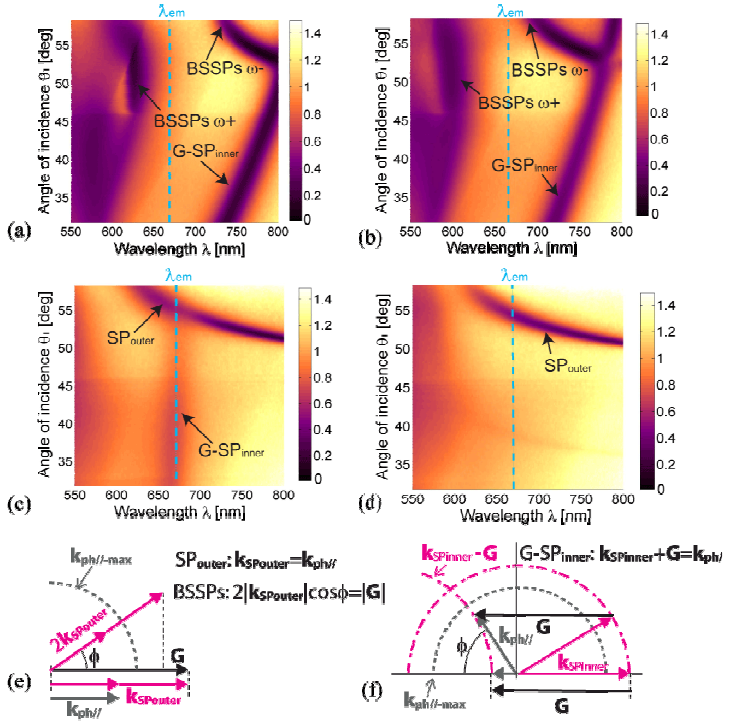

Fig. 8. Azimuth dependence of surface plasmon dispersion relation on a grating with the modulation depth d = 30 nm, Ta_2O_5 layer thickness t_3 = 100 nm, and water medium on the top n_6 = 1.33: (a) ϕ = 0 deg, (b) ϕ = 30 deg, (c) ϕ = 50 deg and (d) ϕ = 90 deg. Polar angles in LaSFN9 glass were measured. Momentum vector scheme for azimuth dependence of (e) Bragg-scaterred SP_{outer} and (f) diffraction grating-coupled SP_{inner}.

In addition, momentum vector schemes are shown in Fig. 8(e)-8(f) in order to illustrate the azimuth dispersion of the coupling to SP_{outer} and SP_{inner}. On the outer surface, the grating was designed to support Bragg-scattered SP_{outer} (occurring when $2\mathbf{k_{SPouter}} = \mathbf{G}$) at the wavelength 670 nm and azimuth angle ϕ = 0. Upon the excitation of SP_{outer} at an increased azimuth angle $\phi > 0$ deg, the parallel component of $2\mathbf{k_{SPouter}}$ to $\mathbf{G}$ is decreased and its magnitude does not match $|\mathbf{G}|$, see Fig. 8(e). In order to fulfill the Bragg-scattering condition, the magnitude of $\mathbf{k_{SPouter}}$ needs to be enlarged which occurs at lower wavelength and leads to

#164156 - $15.00 USD Received 6 Mar 2012; revised 6 Apr 2012; accepted 15 May 2012; published 11 Jun 2012

a blue shift of the bandgap as observed in Fig. 8(a)-8(d). For the inner surface, $SP_{SPinner}$ is excited by −1st diffraction order when the condition $\mathbf{k_{ph}}$-$\mathbf{G}$ = $\mathbf{k_{SPinner}}$ holds (where $\mathbf{k_{ph//}}$ is the in-plane momentum vector of the incident light beam). As Fig. 8(f) shows, the G-SP_{inner} excitation requires an enhanced magnitude of the in-plane momentum of the incident light beam $|\mathbf{k_{ph//}}|$ when the azimuth angle ϕ is increased. This leads to the larger resonance (polar) angle of incidence θ_I at a given wavelength and to a blue shift of the G-SP_{inner} resonance at a fixed angle of incidence θ_I. This trend is in agreement with measured data presented in Fig. 8(a)-8(d).

4.5 SPCE mediated by cross-coupled surface plasmons

Finally, SPCE on the grating structure with cross-coupled surface plasmons at inner and outer metallic surface was studied. The gold grating with the modulation depth of d = 30 nm on BK7 glass substrate was brought in contact with air (n_6 = 1) and water (n_6 = 1.33) in order to tune the SP_{outer}. The refractive index at the inner gold surface was decreased by choosing the thickness of Ta_2O_5 layer t_3 = 0 nm which shifted the excitation of G-SP_{inner} to lower wavelength below 700 nm. For the structure in contact with air, anti-crossing between G-SP_{inner} and ATR-coupled SP_{outer} occurs as seen in the measured dispersion relation in Fig. 9(a). Figure 9(b) shows that for this configuration the SPCE signal at the direction parallel to the grating vector ϕ = 0 and 180 deg is cancelled due to the gap occurring at emission wavelength λ_{em}. In other directions ($\phi \neq 0$ deg), SPCE retains its characteristic circular shape in the same manner with Fig. 8(b). When the refractive index of the upper medium is increased to n_6 = 1.33, the dispersion relation of SP_{outer} shifts to higher angles and a BSSP bandgap opens at wavelengths close to the emission wavelength λ_{em}, see Fig. 9(c).

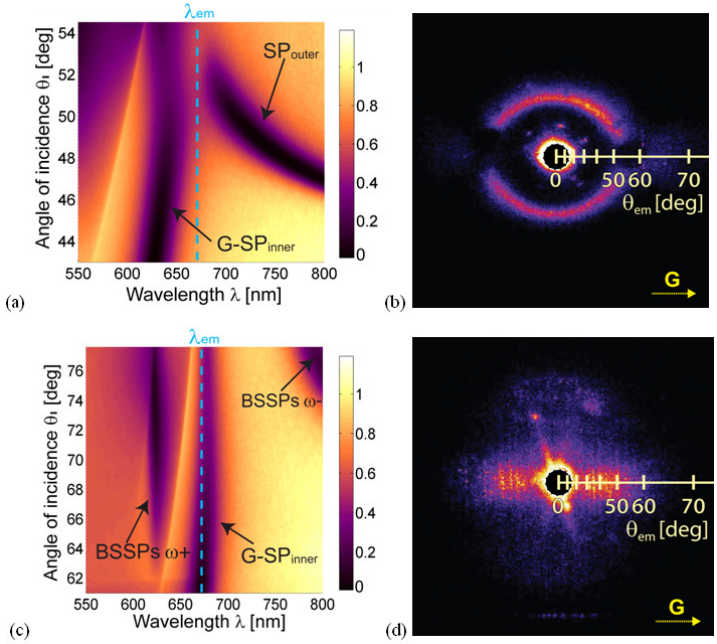

Fig. 9. Dispersion relation of cross-coupled surface plasmon modes for grating with the modulation depth of d = 30 nm and without Ta_2O_5 layer t_3 = 0 nm and the refractive index of upper medium (a) n_6 = 1 and (c) n_6 = 1.33 and respective fluorescence distributions emitted through the substrate (b) and (d).

As discussed in previous section, the grating-coupled SP_{inner} occurring inside this bandgap is partially cross-coupled to BSSPs ω^+ mode (see simulated dispersion relation in Fig. 4(b) which agree well with the experiment and electric field intensity profile in Fig. 5(d)). This

#164156 - $15.00 USD Received 6 Mar 2012; revised 6 Apr 2012; accepted 15 May 2012; published 11 Jun 2012

cross-coupling effect alters the dispersion relation of SP_{inner} which makes the resonance wavelength weakly dependent on the angle of incidence θ_I and increases the field strength at the outer gold interface, see Fig. 5(d). The corresponding SPCE image shows a dominant emission via SP_{inner} centered at azimuth angles $\phi = 0$ and 180 deg and cancelled SPCE cone via SP_{outer} modes. This fluorescence emission pattern has similarity to that shown in Fig. 7(d) for which the emission occurs at higher azimuth angles due to the larger propagation constant of SP_{inner} probing the Ta_2O_5 layer.

5. Conclusions

Dense sub-wavelength plasmonic gratings allow controlling spatial distribution of surface plasmon-coupled emission (SPCE) through a thin metal film on a dielectric substrate. The dispersion relation of surface plasmons at upper and lower interfaces of the thin metallic film can be simply tuned by changing the refractive index at respective metallic interfaces and enables exploiting a rich spectrum of Bragg scattered and cross-coupled surface plasmon modes. These waves can serve as efficient fluorescence decay channels for emitters placed on the top of the metallic film. In particular, modification of surface plasmon characteristics can suppress or enhance the fluorescence light intensity emitted to specific polar and azimuth directions on or inside the characteristic SPCE emission cone. These features can provide means for tuning the interaction of emitters with surface plasmons in areas including optical sources relying on nanoscale antennas and sensor utilizing surface plasmon-enhanced fluorescence spectroscopy. In particular, these observations may provide leads to advance plasmon-enhanced fluorescence sensors through more efficient collecting of fluorescence light emitted via Bragg-scattered surface plasmons, simpler detection of SPCE signal emitted at smaller polar angles and can be useful for multiplexing of sensing channels by emitting the fluorescence light from different sensing areas to different directions.

Acknowledgments

Support for this work was partially provided by the Austrian NANO Initiative (FFG and BMVIT) through the NILPlasmonics project within the NILAustria cluster (www.NILAustria.at) and by the Czech Science Foundation under grant # P205/12/G118.

#164156 - $15.00 USD Received 6 Mar 2012; revised 6 Apr 2012; accepted 15 May 2012; published 11 Jun 2012